Redox Biology 28 (2020) 101355

Contents lists available at ScienceDirect

Redox Biology

journal homepage: www.elsevier.com/locate/redox

# Deletion of *narfl* leads to increased oxidative stress mediated abnormal angiogenesis and digestive organ defects in zebrafish

Jing Luo[a], Xiaokang Zhang[a], Siying He[a], Qiyong Lou[b], Gang Zhai[b], Chuang Shi[b], Zhan Yin[b,*], Fang Zheng[a,**]

[a] Center for Gene Diagnosis, Zhongnan Hospital of Wuhan University, Wuhan, Hubei, 430071, China
[b] State Key Laboratory of Freshwater Ecology and Biotechnology, Institute of Hydrobiology, Chinese Academy of Sciences, Wuhan, Hubei, 430072, China

ARTICLE INFO

*Keywords:*
*Narfl*
Oxidative stress
Angiogenesis
Zebrafish

ABSTRACT

Nuclear prelamin A recognition factor-like (NARFL) is a human protein that participates in cytosolic iron-sulfur (Fe–S) protein biogenesis and cellular defense against oxidative stress. Previous studies of *Narfl* knockout mice did not reveal well the regulatory mechanisms of embryonic development mediated by *Narfl* because the homozygous mice die in utero. Here, we investigated the function of *narfl* in an established zebrafish knockout model by taking advantage of zebrafish external fertilization and ease of embryonic development examination. Our experiments showed that *narfl* deletion resulted in larvae lethality, subintestinal vessel (SIV) malformation and digestive organ defects in the early stages of embryonic development. Biochemical analyses and western blot revealed increased oxidative stress and upregulated hypoxia-inducible factor-1α (HIF-1α) expression in *narfl*$^{-/-}$ fish. The use of HIF-1α inhibitor 2-methoxyestradiol (2ME2) for the treatment of mutants partially rescued the SIV sprouting. These results suggest that *narfl* deletion causes increased oxidative stress and subintestinal vessel malformation, which further influence the development of digestive organs and might contribute to the lethality of the *narfl* knockout fish.

## 1. Introduction

Nuclear prelamin A recognition factor-like (NARFL), also known as cytosolic iron-sulfur assembly component 3 (CIAO3) or iron-only hydrogenase-like protein 1 (IOP1), is a human protein that is homologous to Nar1. Nar1 is an essential component of the cytosolic iron-sulfur (Fe–S) cluster assembly (CIA) pathway in yeast. Fe–S proteins containing [2Fe–2S] and [4Fe–4S] [1,2] participate in many biologic processes, including Krebs cycle reactions, oxidative phosphorylation, translation, iron regulatory pathways and purine metabolism [3]. Previous studies showed that NARFL functions in the cytosolic Fe–S protein biogenesis and knockdown of NARFL causes decreased activity of cytosolic aconitase, an Fe–S protein in mammalian cells [4]. In yeast, genetic deletion of Nar1 is fatal and results in impairment of the cytosolic Fe–S protein assembly [5]. In mice, *Iop1/Narfl* knockout yields intrauterine death and *Iop1* loss in mouse embryonic fibroblasts leads to lethality [6].

It was reported that NARFL knockdown in mammalian cells causes increased levels of hypoxia-inducible factor-1α (HIF-1α) protein under normoxic and hypoxic conditions [7], and recent study has shown that NARFL is a key element in cellular defense against oxidative stress [8]. In our previous work, *NARFL* (Ser161Ile) was identified as a causative gene in a family with diffuse pulmonary arteriovenous malformations (dPAVMs), in which the proband died of pulmonary hypertension at a young age, and we observed abnormal development of the subintestinal vessels using a *narfl*-knockout zebrafish model [9]. Previous studies provide insights regarding the interaction between oxidative stress, angiogenesis and vascular diseases, indicating that oxidative stress plays a positive role during angiogenesis [10–13]. The anti-angiogenic effects of antioxidants also reveal the effects of oxidative stress on angiogenesis and related developmental processes [14–17]. Patricia Siques et al. have summarized that oxidative stress (mainly reactive oxygen species, ROS) participates in the pulmonary vasculature's responses under hypobaric hypoxia, and pointing out that HIF-1α directly induces the activation of NADPH oxidase and contributes to ROS production [18]. In addition, it was reported that oxidative stress contributes to the inactivation of prolyl hydroxylase 2 (PHD2) and results in the stabilization and activation of HIF-1α [19]. These results suggest that ROS and HIF-1α signals are interconnected in vascular development and remodeling, both of which are related to the role of NARFL.

* Corresponding author.
** Corresponding author.
*E-mail addresses:* zyin@ihb.ac.cn (Z. Yin), zhengfang@whu.edu.cn (F. Zheng).

https://doi.org/10.1016/j.redox.2019.101355
Received 2 July 2019; Received in revised form 10 October 2019; Accepted 21 October 2019
Available online 23 October 2019

Therefore, we proposed the present study to explore the function of *narfl* using an established zebrafish model. We observed that all *narfl*-knockout progenies died at 9–18 days post-fertilization (dpf). Mutants demonstrated severe defective development of the subintestinal vessels and digestive organs, increased oxidative stress, upregulated HIF-1α and angiogenesis linked gene expressions. Furthermore, with the treatment of 2-methoxyestradiol (2ME2), an inhibitor of HIF-1α, the subintestinal vessel (SIV) sprouting could be partially rescued in *narfl*$^{-/-}$ fish. Our study provides new insight into the understanding of *narfl* function in oxidative stress and HIF-1α induced angiogenesis from a developmental perspective.

## 2. Materials and methods

### 2.1. Zebrafish maintenance

The wild type zebrafish was maintained in our laboratory under standard conditions [20]. Zebrafish embryos developmental stages were determined by hour post-fertilization (hpf) or dpf [21]. All experiments were performed following the National Guide for the Care and Use of Laboratory Animals and the study was approved by the Institute of Hydrobiology, Chinese Academy of Sciences (Approval ID: IHB 2013724).

### 2.2. Generation of narfl mutant lines and RNA injection

*Narfl* knockout was performed using a CRISPR/Cas9 system as previously described [9]. Homozygous mutants were obtained from F1 embryos that were derived from F0 and wild type intercross. Two mutant lines, namely *narfl*$^{-/-}$-1 (harboring 4 bp insertion) and *narfl*$^{-/-}$-2 (harboring 5 bp deletion plus 4 bp insertion), were genotype-identified using primers shown in Table S1 in supplementary information. For *narfl* mRNA injection, full length of zebrafish *narfl* cDNA was cloned into pSP64-poly A vector and synthesized into the capped mRNA using a mMESSAGE mMACHINE SP6 Kit (Ambion, Austin, TX, USA). About 300 ng/μL *narfl* mRNA was injected into 1–2 cell stage embryos.

### 2.3. Reverse transcription PCR (RT-PCR) and quantitative real time PCR (qPCR)

Total RNA was extracted from the embryos at different developmental stages and adult tissues using the Trizol reagent (Invitrogen, Carlsbad, CA, USA). The cDNA was synthesized using the RevertAid First Strand cDNA Synthesis Kit (Thermo Scientific, Waltman, MA, USA) following the standard instructions. Transcript levels of *narfl* at different embryonic stages and adult tissues in wild type fish were analyzed using RT-PCR. The qPCR was performed using the AceQ qPCR SYBR Green Master Mix (Vazyme, Nanjing, China). Data were analyzed using a △△Ct method and *β-actin 1* served as the house-keeping gene. All the experiments were performed in triplicate and the primers are listed in Supplementary Table S1.

### 2.4. RNA-seq analysis

Total RNA was isolated from 4 dpf *narfl*$^{+/+}$ and *narfl*$^{-/-}$ larvae using the Trizol reagent following the standard protocols. About 100 bp paired-end reads were obtained by sequencing on the Illumina (HiSeq 2500/4000) platform. After removing adaptor sequences and low-quality sequences, the remaining paired-end clean reads were aligned to zebrafish genome using TopHat v2.0.12. Normalized gene expression level was separately calculated as Fragments per Kilobase of transcript per Million fragments mapped (FPKM). The cutoff value was determined based on a 95% confidence interval for all the FPKM values to evaluate gene transcriptional activity.

### 2.5. Whole-mount in situ hybridization

Whole-mount *in situ* hybridization of anti-sense RNA probes, including *narfl*, *fabp1a* (liver probe), *fabp2* (intestine probe), *ela2l* (exocrine pancreas probe) and *hif1ab*, was performed as previously described [22–24].

### 2.6. Alkaline phosphatase staining and confocal imaging

Embryos were fixed overnight in 4% paraformaldehyde and processed for alkaline phosphatase staining as previously described [25]. The *fli*:GFP/*narfl*$^{-/-}$ homozygous lines were generated by mating the *fli*:GFP/*narfl*$^{+/-}$ adult fish, which were obtained by hybridizating the *fli*:GFP/Con and *narfl*$^{+/-}$ fish. Confocal images of 3 dpf transgenic embryos were generated using a Zeiss ISM 710 confocal microscope.

### 2.7. Western blot

Protein extracts were subjected to 8%–12% SDS-PAGE and transferred to the PVDF membrane (Millipore, Hayward, CA, USA). Rabbit anti-NARFL (1:1000, Abclonal, Wuhan, China), rabbit anti-HIF-1α (1:500, Boster, Wuhan, China), rabbit anti-Akt (1:1000, Cell Signaling Technology, MA, USA), rabbit anti-phosphorylated Akt (1:1000, Cell Signaling Technology, MA, USA), mouse anti-β-Actin (1:1000, Santa Cruz Biotechnology, Santa Cruz, CA, USA) were used as the primary antibodies. The secondary antibodies conjugated to horseradish peroxidase were used at 1:5000 dilutions (proteintech, Wuhan, China).

### 2.8. ROS assay

Caudal fins of embryos were cut for genomic DNA isolation and genotyping using the NaOH lysis method as previously described [26]. After the fish tail genotyping, the rest of the body was sampled for ROS assay based on an established method [27]. Briefly, embryo was digested with 100 μL of 0.25% (w/v) trypsin/EDTA solution for 10 min before 200 μL of DMEM containing 10% (v/v) fetal bovine serum (FBS) was added to stop the reaction. Then sample was centrifuged at 2500 rpm for 5 min at 4 °C to remove the supernatant, and cell pellet was washed in 200 μL of PBS containing 2% (v/v) FBS. After centrifugation again, cells were resuspended in 200 μL of PBS containing 2% FBS with 10 μM DCFH-DA probe (Beyotime, Nanjing, China) and incubated at 37 °C for 30 min. Sample without probe incubation was served as a negative control. Fluorescence was detected at the excitation/emission wavelength of 488/525 nm using a FACSCanto Flow Cytometer (BD Bioscience, USA). To inhibit the ROS level, 1 mM N-acetylcysteine [27] (NAC, Sigma-Aldrich, St. Louis, MO, USA) was used for antioxidant exposure from 24 hpf, then 3 dpf embryos were collected for ROS measurement after two days of treatment.

### 2.9. Biochemical analyses

Cytosolic aconitase activity was determined using an Aconitase Activity Assay Kit (Sigma-Aldrich, St. Louis, MO, USA). Cellular redox substances including superoxide dismutase (SOD), glutathione sulfur transferase (GST), glutathione (GSH), and malondialdehyde (MDA) were detected by colorimetry using commercially available assay kits (Beyotime, Nanjing, China). All assays were implemented with three replications.

### 2.10. Drug exposure

Embryos were exposed to drug at 24 hpf before the first sprouts form the first subintestinal venous plexus vessel [28]. Because the endogenous alkaline phosphatase activity reaches a relatively high level at 3 dpf, and the subintestinal venous plexus starts regressing at 4 dpf, thus 3 dpf embryos were collected for subsequent testing after two days

of treatment. Embryos were dechorionated at 24 hpf and distributed on a 6-well plate (20 embryos per well) for drug exposure. The 2ME2 (Selleck, Houston, TX, USA) used in the experimental group was 0.2 μM or 2 μM and the control group was treated with dimethylsulfoxide (DMSO) at the same concentration used in 2ME2 treated fish (See the Supplementary Fig. S1 for drug concentration selection).

### 2.11. Statistical analyses

Student's t tests were used for statistical analyses with SPSS 20.0 (SPSS Inc., Chicago, USA). All data were expressed as the mean and standard deviation (mean ± SD). Results were considered significant when the probability of making a type I error was less than 5% ($P < 0.05$).

## 3. Results

### 3.1. Expression patterns of narfl in wild type fish and generation of narfl mutant lines

RT-PCR results showed that *narfl* was widely expressed in the early stages of embryonic development (Fig. 1A) and adult tissues, including brain, gill, eye, heart, liver, spleen, muscle, kidney and intestine (Fig. 1B). The spatio-temporal expression patterns provided by whole-mount *in situ* hybridization showed that *narfl* was expressed in liver and intestine at 3 dpf and the expression increased over time (Fig. 1C–H).

CRISPR/Cas9-mediated *narfl* knockout was described in our previous work [9]. Two independent mutant lines, respectively containing 4 bp insertion and 5 bp deletion plus 4 bp insertion in the target region, were obtained and confirmed by sequencing (Fig. 1I). Compared with the wild type *narfl* that encoded a protein of 477 amino acids, the putative translation products with premature stop codons of the two mutant lines contained 198 and 221 amino acid residues, respectively. The cytosolic aconitase activity was diminished in *narfl*$^{-/-}$ fish compared with the control siblings (Fig. 1J). Western blot revealed obviously decreased NARFL protein levels in mutant lines (Fig. 1K-L). In addition, we examined the expressions of *narfl* and *narfl* associated genes such as *ciao1*, *rsad2* and *ciao2a*, and the qPCR results are presented in Supplementary Fig. S2.

### 3.2. Larvae lethality and subintestinal vessel malformation in narfl$^{-/-}$ fish

The *narfl* knockout resulted in zebrafish larvae death from 9 to 18 dpf (Fig. 2A). Alkaline phosphatase staining of 3 dpf embryos showed maldevelopment of subintestinal vessels in *narfl*$^{-/-}$ fish (Fig. 2B–D). The confocal images of *fli*:GFP/*narfl*$^{+/-}$ offsprings revealed subintestinal

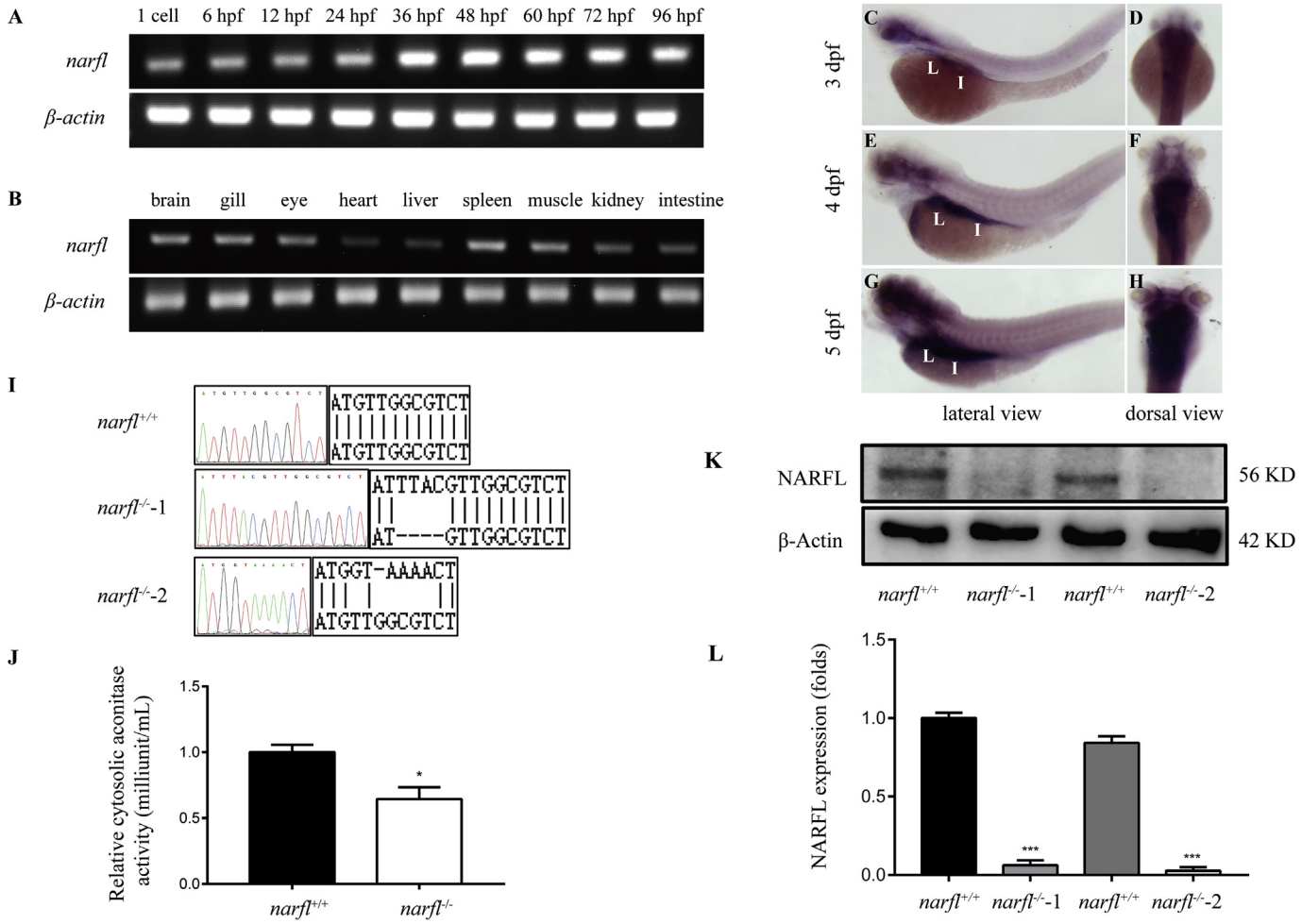


**Fig. 1. Expression patterns of *narfl* in wild type fish and generation of *narfl*-knockout lines. A-B**: RT-PCR evaluated the expression patterns of wild type zebrafish *narfl* gene at different embryonic stages (**A**) and in various adult tissues (**B**). **C–H**: Spatio-temporal expression pattern analysis of *narfl* with whole-mount *in situ* hybridization in wild type fish. **C**, **E** and **G**: Lateral view anterior to the left. **D**, **F** and **H**: Dorsal view anterior to the top. L: liver. I: intestine. **I**: DNA sequences of *narfl*$^{+/+}$ and *narfl*$^{-/-}$ zebrafish. The *narfl*$^{-/-}$-1 represented a mutant line containing 4 bp insertion and *narfl*$^{-/-}$-2 represented a mutant line containing 5 bp deletion plus 4 bp insertion. **J**: Relative cytosolic aconitase activity measured in *narfl*$^{+/+}$ and *narfl*$^{-/-}$ fish. **K-L**: Western blot analysis of NARFL protein in mutants and control siblings. *, $P < 0.05$, ***, $P < 0.001$.

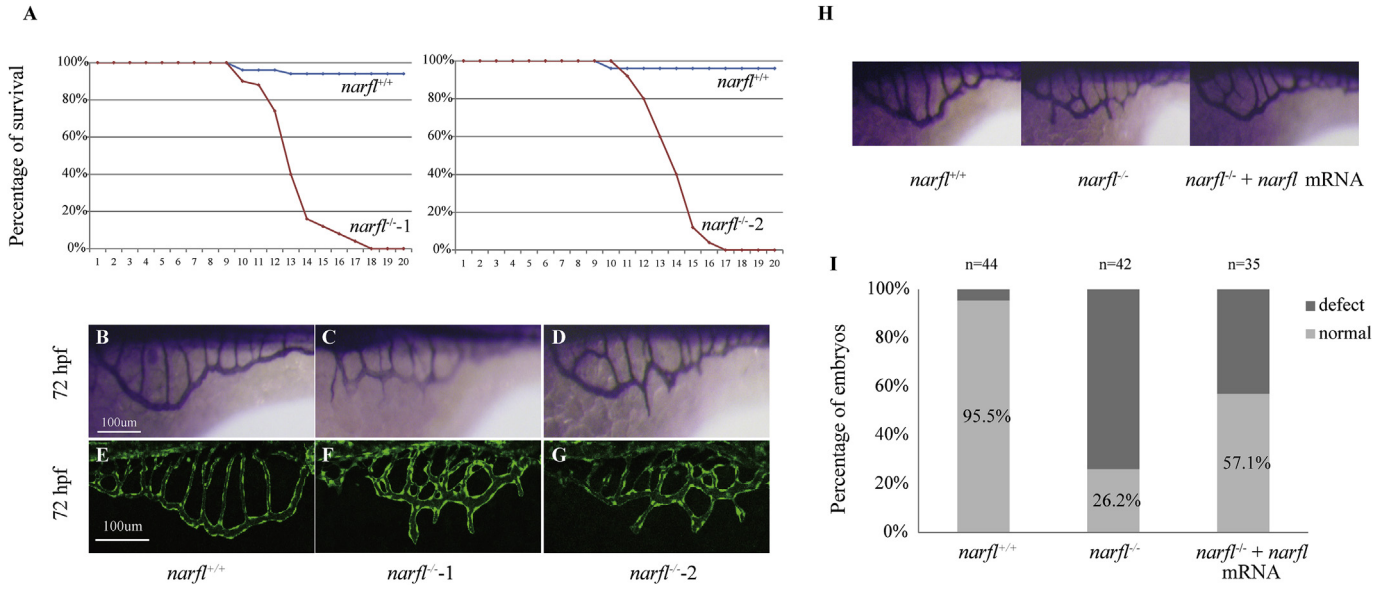


**Fig. 2. The *narfl* deletion impaired subintestinal vessel development and zebrafish survival. A**: Survival rate statistics. **B-D**: Alkaline phosphatase staining of *narfl*$^{+/+}$ and *narfl*$^{-/-}$ embryos at 72 hpf. **E-G**: Confocal images of *fli*:GFP/*narfl*$^{+/+}$ and *fli*:GFP/*narfl*$^{-/-}$ larvae at 72 hpf. **H–I**: Statistics of subintestinal vessel defect rates in *narfl*$^{+/+}$, *narfl*$^{-/-}$ larvae and *narfl*$^{-/-}$ larvae injected with zebrafish *narfl* mRNA. The "n" represents the number of embryos counted.

vascular abnormal sprouting in *fli*:GFP/*narfl*$^{-/-}$ larvae (Fig. 2E–G). Wild type zebrafish *narfl* mRNA was synthesized and injected into 1–2 cell stage *narfl*$^{-/-}$ embryos and the defective phenotype of subintestinal vessels was partially rescued (Fig. 2H-I).

### 3.3. Disturbed signaling pathways including increased angiogenesis and glycolysis signals in *narfl*$^{-/-}$ fish

We performed transcriptome analysis of *narfl*$^{+/+}$ and *narfl*$^{-/-}$ larvae at 4 dpf using RNA sequencing. The differentially expressed genes between wild type and mutant fish were highly involved in metabolic pathway and fat digestion and absorption pathway. Genes associated with glycolysis (e.g. *hkdc1*, *aldoca*, *gck*, *pgk1* and *slc2a1a*) and angiogenesis (e.g. *vegfaa*, *kdr*, *pdgfra*, *angpt1*, *tek*, *tgfb2* and *tgfbr2*), especially genes in the Bmp pathway (e.g. *bmp2b*, *bmp4*, *bmp7b* and *bmp16*) were upregulated in *narfl*$^{-/-}$ fish. The qPCR results verified the increased expression of some of the above genes and other angiogenesis associated genes (*vegfab* and *pdgfrb*) chosen based on previous studies [29–36] (Supplementary Fig. S3). The *fabp1b.1*, *fabp2* and *apoa4b.2* genes involved in fat digestion and absorption pathway, and *ela2*, *ela2l* and *try* genes involved in pancreatic secretion were downregulated in *narfl*$^{-/-}$ fish. Data are presented in Supplementary Table S2.

### 3.4. Maldevelopment of digestive organs in *narfl*$^{-/-}$ fish

Reduced food intake was observed in *narfl*$^{-/-}$ larvae compared with the control siblings (Fig. 3A). *In situ* hybridization of liver probe (*fabp1a*), intestine probe (*fabp2*), and exocrine pancreas probe (*ela2l*) at 4 dpf showed decreased signal expression in mutants (Fig. 3B–J), as confirmed by qPCR data (Fig. 3K). This was consistent with the downregulated genes involved in fat digestion and absorption as well as pancreatic secretion in the transcriptome data (Supplementary Table S2).

### 3.5. Increased oxidative stress and upregulated HIF-1α protein expression in *narfl*$^{-/-}$ fish

In *narfl*$^{-/-}$ fish, we observed significantly elevated ROS level ($P < 0.001$), which could be downregulated after NAC treatment, compared with the wild type fish (Fig. 4A–C). The cytosolic SOD activity and GST activity were diminished in *narfl*$^{-/-}$ fish (Fig. 4D-E). Cytosolic content of GSH was decreased, while the MDA content had the increasing tendency but was not significantly affected in mutants (Fig. 4F-G). The result of *in situ* hybridization of 4 dpf larvae showed increased expression of *hif1ab* in mutants (Fig. 4H). This was confirmed by western blot result, which revealed upregulated HIF-1α protein level in *narfl*$^{-/-}$ fish (Fig. 4I-J). In addition, we observed increased phosphorylated Akt (p-Akt) protein level in mutant fish, as determined by western blot analysis (Fig. 4I–K).

### 3.6. The 2ME2 partially inhibited SIV sprouting and activated pathways induced by HIF-1α in *narfl*$^{-/-}$ fish

The *narfl*$^{+/+}$ and *narfl*$^{-/-}$ fish were treated with HIF-1α inhibitor 2ME2 at 24 hpf, and 3 dpf embryos were sampled for alkaline phosphatase staining and RNA extraction. The results showed that 2ME2 treatment partially inhibited SIV sprouting in *narfl*$^{-/-}$ fish (Fig. 5A-B). The upregulated expressions of genes involved in glycolysis signaling pathways (including *hkdc1*, *aldoca*, *gck*), and in angiogenesis linked pathways (including *bmp2b*, *bmp7b*, *bmp16*, *vegfab*, *kdr*, *pdgfrb*, *angpt1* and *tek*) in the *narfl* knockout fish were all inhibited (Fig. 5C-M).

## 4. Discussion

In the present study, the knockout of *narfl* in zebrafish resulted in decreased aconitase activity and larvae lethality. In *narfl*$^{-/-}$ fish, we observed defective development of subintestinal vessels, increased oxidative stress and HIF-1α expression. Using HIF-1α inhibitor 2ME2 for treatment partially rescued the subintestinal vascular sprouting in mutants, and suppressed the upregulated expressions of genes involved in angiogenesis and glycolysis signals. These results indicate that *narfl* knockout activated ROS-HIF-1α signal and mediated abnormal sprouting of subintestinal vessels, which led to digestive organ maldevelopment and probably larvae lethality.

The oxidative stress was increased and HIF-1α expression was upregulated in *narfl* knockout fish, which were consistent with the findings in mammalian cells [7,8]. In normoxic condition, HIF-1α is mainly hydroxylated by PHD2 in the presence of $O_2$, $Fe^{2+}$ and 2-oxoglutarate (2-OG), and undergoes proteasomal degradation finally [37,38]. Previous research demonstrated that the stabilization and activation of

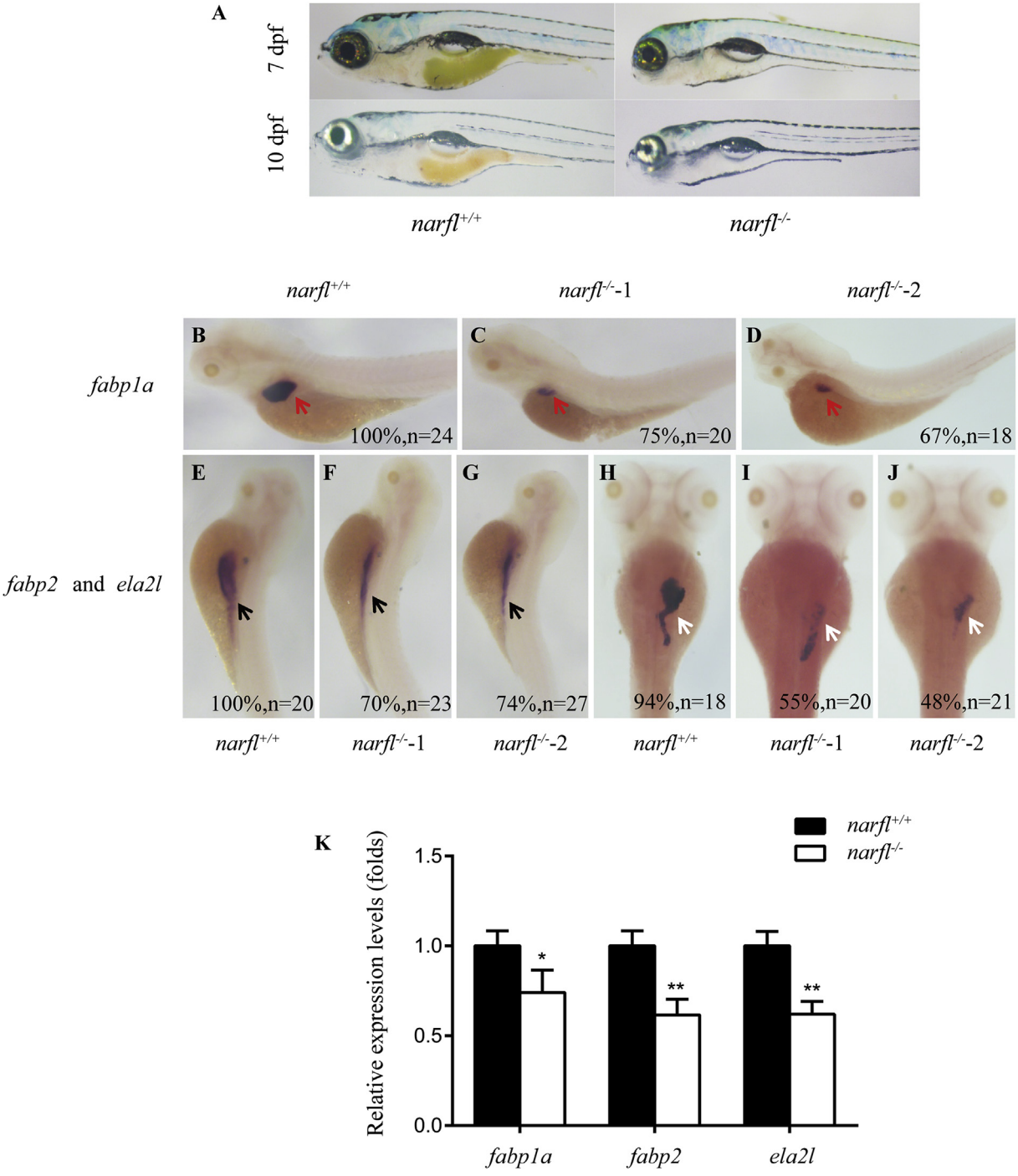


**Fig. 3. Zebrafish *narfl* deletion induced defective development of digestive organs. A**: Food intake 30 min after 7 dpf larvae fed with egg yolk and 10 dpf larvae with fairy shrimp. Larvae were imaged using a dissection microscope. **B-J**: *In situ* hybridization of *fabp1a* (**B-D**), *fabp2* (**E-G**), and *ela2l* (**H-J**) at 4 dpf. Red arrowheads indicate the liver, black arrowheads indicate the intestine and white arrowheads indicate the exocrine pancreas. For *in situ* hybridization results, at least 18 embryos per genotype were analyzed in two separated experiments. **K**: The qPCR result of *fabp1a*, *fabp2* and *ela2l* genes in $narfl^{-/-}$ fish and control siblings. *, $P < 0.05$, **, $P < 0.01$. (For interpretation of the references to color in this figure legend, the reader is referred to the Web version of this article.)

HIF-1α were regulated by PHD2, an Fe(II)-dependent dioxygenase that could be inactivated by oxidative stress [19]. In our previous study, we found that NARFL expression was decreased and ferric iron was accumulated in the dPAVMs patient's lung tissue [9]. Therefore, it is conceivable that *NARFL* knockout causes abundant ferric iron but a deficiency of ferrous iron, and thus inactivates PHD2. Furthermore, ROS was reported to independently play a positive role in the upregulation of HIF-1α concentration under normal circumstances [39–42], which implies that increased ROS may directly activate HIF-1α in $narfl^{-/-}$ fish. In a previous study of gastrointestinal vascular malformation (GIVM), it was reported that abnormally high expression of HIF-1α and HIF-2α could cause GIVM through inducing angiogenesis and SIV sprouting in zebrafish, which is similar to the phenotype observed in our $narfl^{-/-}$ fish [43]. Referring to the angiogenesis during zebrafish embryo development, Vegf, Notch and Bmp signals were all reported to be involved in the subintestinal venous plexus development [28,44]. Vegf promoted the sprouting of the predominantly venous plexus and Bmp promoted the outgrowth of the structure, but whether Notch

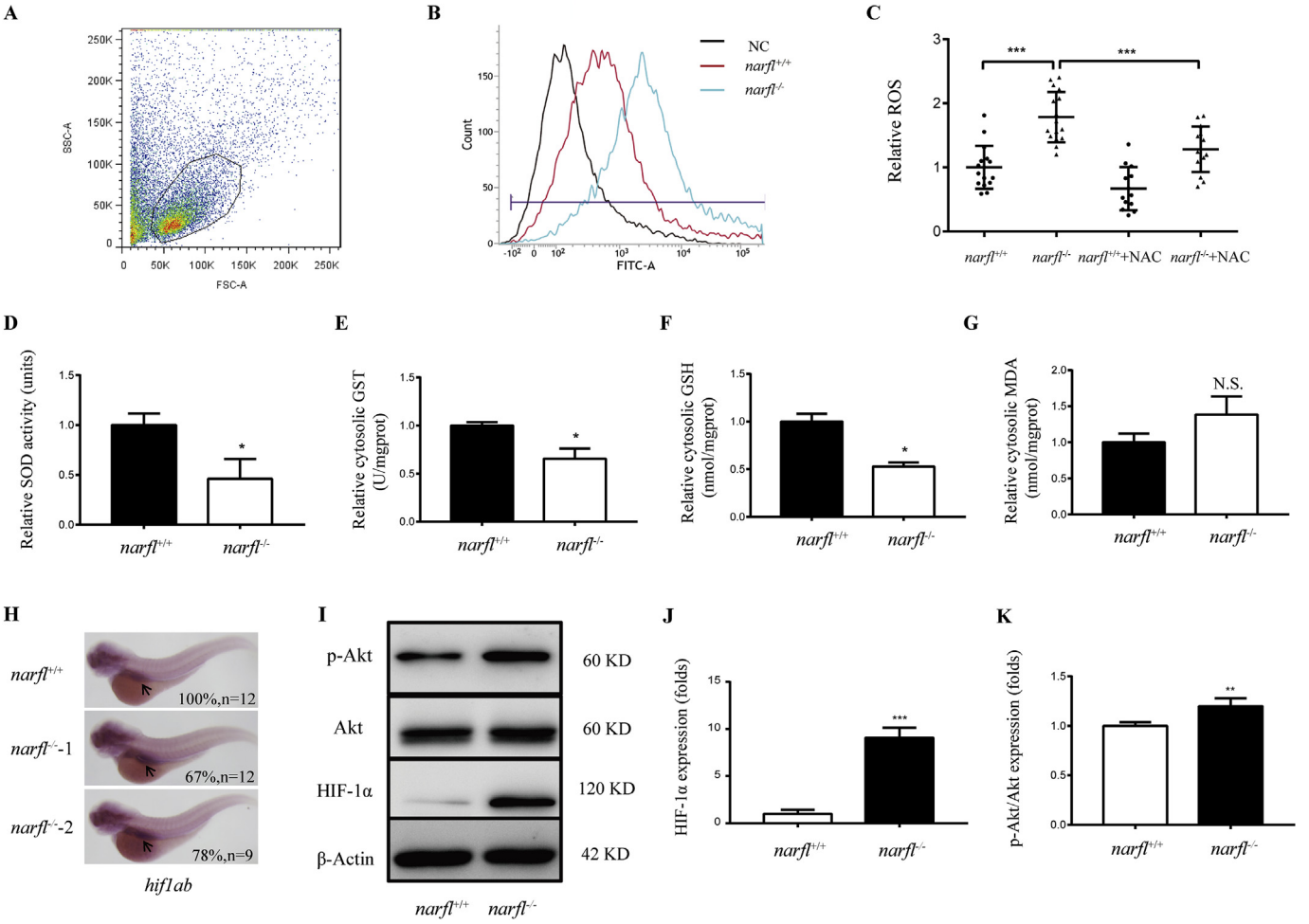


**Fig. 4. Increased oxidative stress and HIF-1α expression in *narfl*$^{-/-}$ zebrafish.** **A**: Flow cytometry gating of a single-cell suspension created from zebrafish embryos (Intact cells were gated by forward scatter (FSC) and side scatter (SSC) properties). **B**: Representative flow cytometry histograms showing DCFH-DA emission in 3 dpf *narfl*$^{+/+}$ and *narfl*$^{-/-}$ fish. NC, negative control. **C**: ROS contents detected by flow cytometry in control siblings and mutants before and after NAC treatment. **D-G**: Relative cytosolic activities of SOD (**D**) and GST (**E**) as well as GSH (**F**) and MDA (**G**) contents in *narfl*$^{+/+}$ and *narfl*$^{-/-}$ fish. **H**: *In situ* hybridization of *hif1ab* at 4 dpf. Black arrowheads indicate the HIF-1α signal in intestine area, and at least 9 embryos per genotype were analyzed in two separated experiments. **I**: Western blot analysis of HIF-1α, Akt and p-Akt protein levels in mutants and control siblings. **J**: Western blot of HIF-1α expressions quantified using gray value analysis with Image J software. **K**: Western blot of p-Akt/Akt expressions quantified using gray value analysis with Image J software. *, $P < 0.05$, **, $P < 0.01$, ***, $P < 0.001$, N.S., no significance.

signal worked in this process remains controversial [28,44]. In addition, previous investigations of cultured rat sympathetic neurons showed that ROS was involved in BMP-induced dendritic growth [45]. In a study of fibrodysplasia ossificans progressiva, HIF-1α was found to play a positive role in the hypoxic amplification of BMP signaling in the endosomal compartment of hypoxic connective tissue progenitor cells [46]. Therefore, we speculate whether ROS induced HIF-1α activation and mediated the SIV sprouting through angiogenesis linked pathways especially the Bmp signaling in *narfl*$^{-/-}$ fish. Correspondingly, both the RNA-seq and qPCR results showed that genes involved in Bmp pathway, including *bmp2b*, *bmp7b* and *bmp16*, were upregulated in mutant fish. Using 2ME2 for HIF-1α inhibition, the SIV sprouting in mutants was partially rescued and the increased expressions of Bmp-related and other angiogenesis linked genes were suppressed. These results suggest that Bmp signaling is dominantly involved in ROS-HIF-1α-induced subintestinal vessel malformation in zebrafish. Taken together, we conclude that knocking out zebrafish *narfl* causes increased oxidative stress, which activates Bmp signaling and results in SIV sprouting, as shown in the functional mechanism diagram of *narfl* in Fig. 6.

Zebrafish subintestinal plexus is a set of venous angiogenic vessels that absorb nutrients from the yolk and deliver them to the adjacent yolk syncytial layer, which later supports the distribution of blood to the digestive system [47,48]. This plexus comprises vessels that vascularize the gut, liver and pancreas, and is considered as an ideal model to investigate organ-specific vessel formation [44]. We performed a series of *in situ* hybridization using probes against the digestive organs, and noticed that the liver, intestine and exocrine pancreas were smaller in *narfl*$^{-/-}$ fish. Feeding experiments revealed that food intake in mutants was significantly less compared with the control siblings. All these information suggests that malformation of subintestinal vessels in *narfl*-knockout fish might retard the organ-specific vessel formation to impair the normal development of digestive organs.

In the present study, we utilized a *narfl*-knockout zebrafish model with the subintestinal vessel disorder and demonstrated that *narfl* was essential for embryonic development and organism defense against oxidative stress. We conclude that increased oxidative stress induced by *narfl* deletion disturbs the development of subintestinal vessels and digestive organs through the ROS-HIF-1α-Bmp pathway, and may contribute to the death of *narfl*$^{-/-}$ fish. In our previous study, NARFL was identified as a possible genetic basis underlying dPAVMs [9], and in the present study, *narfl* knockout led to an abnormal angiogenic phenotype in zebrafish. In fact, oxidative stress was reported to be

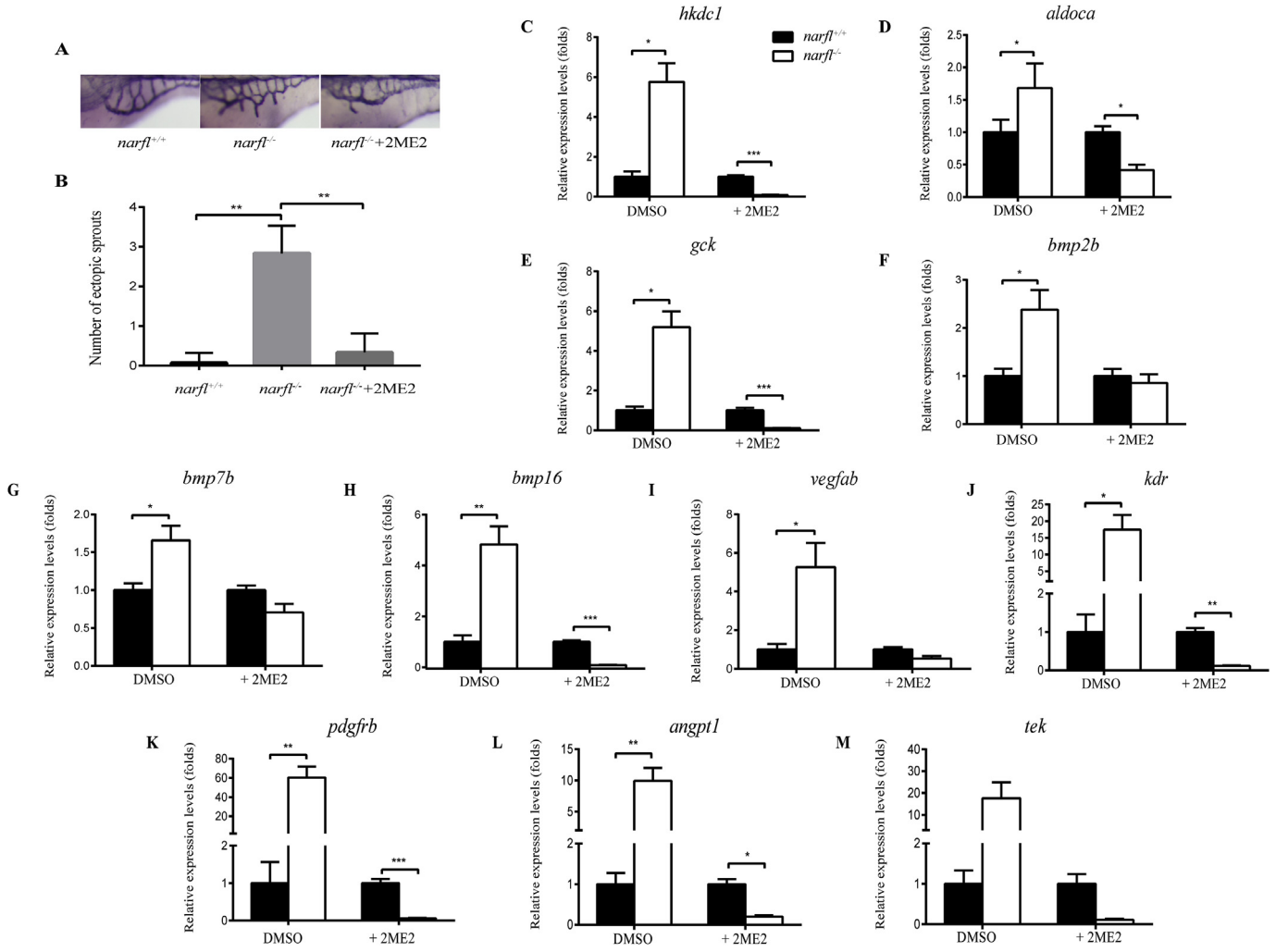


**Fig. 5. The 2ME2 treatment rescued the subintestinal vessel defect. A-B**: Alkaline phosphatase staining statistics for 3 dpf embryos treated with 0.2 μM 2ME2. Data are presented from three independent experiments in which at least 30 embryos per group were analyzed. **C-M**: The qPCR analyses of *hkdc1*, *aldoca*, *gck*, *bmp2b*, *bmp7b*, *bmp16*, *vegfab*, *kdr*, *pdgfrb*, *angpt1* and *tek* in *narfl*$^{+/+}$ and *narfl*$^{-/-}$ fish after two days of 2 μM 2ME2 treatment. *, $P < 0.05$, **, $P < 0.01$, ***, $P < 0.001$.

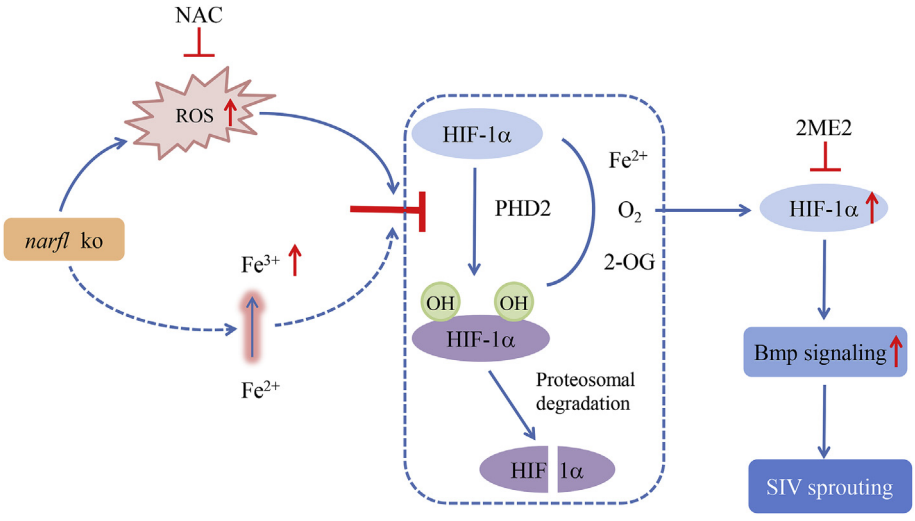


**Fig. 6. Hypothetical schema for *narfl* deletion-induced oxidative stress mediated abnormal angiogenesis in zebrafish.** Solid lines indicate the pathways revealed by previous studies and our research, and dotted lines represent the hypothesis part. Dotted box indicates the proteosomal degradation process of HIF-1α.

closely associated with the development of pulmonary vascular disease and pulmonary hypertension [49–52]. Therefore, our observation of the abnormal angiogenesis mediated by increased oxidative stress in a *narfl* knockout zebrafish model provides evidence for a deeper understanding of the pathological mechanism of cytosolic iron-sulfur assembly component involved in vascular remodeling of pneumonosis.

It is worth noting that both NAC and 2ME2 treatments failed to rescue the lethal phenotype caused by *narfl* knockout (data not shown). Possible speculations include: 1) in addition to the ROS signal, there might be other potential mechanisms through which *narfl* affects embryonic development; 2) the mode of drug administration could not properly balance the effects of ROS due to the inability to distinguish the harmful effects of excessive ROS and the physiological ROS-mediated processes [53,54]. Detailed functional studies of NARFL in other cytological and mammalian experimental systems seem necessary, and it would be challenging to investigate whether NARFL is responsible for any other developmental processes apart from our proposed regulatory network in the present study.

## Declaration of competing interest

The authors declare no conflicts of interest.

## Acknowledgments

This work was supported by grants from the National Natural Science Foundation of China (No. 81472024 and No. 81871722).

## Appendix A. Supplementary data

Supplementary data to this article can be found online at https://doi.org/10.1016/j.redox.2019.101355.

## References

[1] R. Lill, Function and biogenesis of iron–sulphur proteins, Nature 460 (2009) 831.
[2] H. Ye, T.A. Rouault, Human Iron−Sulfur cluster Assembly, cellular iron homeostasis, and disease, Biochemistry 49 (2010) 4945–4956.
[3] T.A. Rouault, W.-H. Tong, Iron–sulphur cluster biogenesis and mitochondrial iron homeostasis, Nat. Rev. Mol. Cell Biol. 6 (2005) 345.
[4] D. Song, F.S. Lee, A role for IOP1 in mammalian cytosolic iron-sulfur protein biogenesis, J. Biol. Chem. 283 (2008) 9231–9238.
[5] J. Balk, A.J. Pierik, D.J.A. Netz, U. Mühlenhoff, R. Lill, The hydrogenase-like Nar1p is essential for maturation of cytosolic and nuclear iron–sulphur proteins, EMBO J. 23 (2004) 2105.
[6] D. Song, F.S. Lee, Mouse knock-out of IOP1 protein reveals its essential role in mammalian cytosolic iron-sulfur protein biogenesis, J. Biol. Chem. 286 (2011) 15797–15805.
[7] J. Huang, et al., IOP1, a novel hydrogenase-like protein that modulates hypoxia-inducible factor-1α activity, Biochem. J. 401 (2007) 341.
[8] M.V. Corbin, D.A.P. Rockx, A.B. Oostra, H. Joenje, J.C. Dorsman, The iron-sulfur cluster assembly network component NARFL is a key element in the cellular defense against oxidative stress, Free Radic. Biol. Med. 89 (2015) 863–872.
[9] H.-Z. Liu, et al., A novel mutation in nuclear prelamin a recognition factor-like causes diffuse pulmonary arteriovenous malformations, Oncotarget 8 (2016) 2708–2718.
[10] Y.-W. Kim, T.V. Byzova, Oxidative stress in angiogenesis and vascular disease, Blood 123 (2014) 625.
[11] Y.-J. Huang, G.-X. Nan, Oxidative stress-induced angiogenesis, J. Clin. Neurosci. 63 (2019) 13–16.
[12] D. Xian, et al., Emerging roles of redox-mediated angiogenesis and oxidative stress in dermatoses, Oxidative Med. Cell. Longevity 2019 (2019) 2304018.
[13] T. Münzel, et al., Impact of oxidative stress on the heart and vasculature: Part 2 of a 3-Part Series, J. Am. Coll. Cardiol. 70 (2017) 212–229.
[14] Y.M. Kim, K.E. Kim, G.Y. Koh, Y.-S. Ho, K.-J. Lee, Hydrogen peroxide produced by angiopoietin-1 mediates angiogenesis, Cancer Res. 66 (2006) 6167.
[15] S. Garrido-Urbani, et al., Targeting vascular NADPH oxidase 1 blocks tumor angiogenesis through a PPARα mediated mechanism, PLoS One 6 (2011) e14665.
[16] S. Coso, et al., NADPH oxidases as regulators of tumor angiogenesis: current and emerging concepts, Antioxidants Redox Signal. 16 (2012) 1229–1247.
[17] L. Bräutigam, et al., MGST1, a GSH transferase/peroxidase essential for development and hematopoietic stem cell differentiation, Redox Biol. 17 (2018) 171–179.
[18] P. Siques, J. Brito, E. Pena, Reactive oxygen species and pulmonary vasculature during hypobaric hypoxia, Front. Physiol. 9 (2018) 865-865.
[19] G. Lee, et al., Oxidative dimerization of PHD2 is responsible for its inactivation and contributes to metabolic reprogramming via HIF-1α activation, Sci. Rep. 6 (2016) 18928.
[20] G. Song, et al., Deletion of Pr72 causes cardiac developmental defects in Zebrafish, PLoS One 13 (2018) e0206883.
[21] C.B. Kimmel, W.W. Ballard, S.R. Kimmel, B. Ullmann, T.F. Schilling, Stages of embryonic development of the zebrafish, Dev. Dynam. 203 (1995) 253–310.
[22] C. Moens, Whole mount RNA in situ hybridization on zebrafish embryos: hybridization, Cold Spring Harb. Protoc. 2008 (2008) pdb.prot5037.
[23] C. Moens, Whole mount RNA in situ hybridization on zebrafish embryos: mounting, Cold Spring Harb. Protoc. 2008 (2008) pdb.prot5038.
[24] C. Moens, Whole mount RNA in situ hybridization on zebrafish embryos: probe synthesis, Cold Spring Harb. Protoc. 2008 (2008) pdb.prot5036.
[25] L. Li, D. Chen, X. Tu, Q. Wang, Z. Yin, Functional characterization of Klippel–Trenaunay syndrome gene AGGF1 identifies a novel angiogenic signaling pathway for specification of vein differentiation and angiogenesis during embryogenesis, Hum. Mol. Genet. 22 (2012) 963–976.
[26] N.D. Meeker, S.A. Hutchinson, L. Ho, N.S. Trede, Method for isolation of PCR-ready genomic DNA from zebrafish tissues, Biotechniques 43 (2007) 610–614.
[27] A.C. Kramer, et al., TP53 modulates oxidative stress in Gata1(+) erythroid cells, Stem Cell Rep. 8 (2017) 360–372.
[28] M. Goi, S.J. Childs, Patterning mechanisms of the sub-intestinal venous plexus in zebrafish, Dev. Biol. 409 (2016) 114–128.
[29] F. Shigetomo, et al., Angiopoietin-1/Tie2 receptor signaling in vascular quiescence and angiogenesis, Histol. Histopathol. 25 (2010).
[30] W.-L. Kwong, et al., A macrocyclic Ruthenium(III) complex inhibits angiogenesis with down-regulation of vascular endothelial growth factor receptor-2 and suppresses tumor growth in vivo, Angew. Chem. Int. Ed. 55 (2016) 13524–13528.
[31] Z.-M. Fan, et al., Dalbergia odorifera extract promotes angiogenesis through upregulation of VEGFRs and PI3K/MAPK signaling pathways, J. Ethnopharmacol. 204 (2017) 132–141.
[32] Y. Onogi, et al., PDGFRβ regulates adipose tissue expansion and glucose metabolism via vascular remodeling in diet-induced obesity, Diabetes 66 (2017) 1008.
[33] J. Liu, et al., IL-33 initiates vascular remodelling in hypoxic pulmonary hypertension by up-regulating HIF-1α and VEGF expression in vascular endothelial cells, EBioMedicine 33 (2018) 196–210.
[34] G.N. Yin, et al., Pericyte-derived Dickkopf2 regenerates damaged penile neurovasculature through an Angiopoietin-1-Tie2 pathway, Diabetes 67 (2018) 1149.
[35] W. Wu, et al., Chronic intermittent hypoxia accelerates liver fibrosis in rats with combined hypoxia and nonalcoholic steatohepatitis via angiogenesis rather than endoplasmic reticulum stress, Acta Biochim. Biophys. Sin. 51 (2019) 159–167.
[36] L. Yang, et al., MicroRNA-26b-5p inhibits mouse liver fibrogenesis and angiogenesis by targeting PDGF receptor-beta, Mol. Ther. Nucleic Acids 16 (2019) 206–217.
[37] G.N. Masoud, W. Li, HIF-1α pathway: role, regulation and intervention for cancer therapy, Acta Pharm. Sin. B 5 (2015) 378–389.
[38] L. Singh, S. Aldosary, A.S. Saeedan, M.N. Ansari, G. Kaithwas, Prolyl hydroxylase 2: a promising target to inhibit hypoxia-induced cellular metabolism in cancer cells, Drug Discov. Today 23 (2018) 1873–1882.
[39] T. Kietzmann, A. Görlach, Reactive oxygen species in the control of hypoxia-inducible factor-mediated gene expression, Semin. Cell Dev. Biol. 16 (2005) 474–486.
[40] R.S. BelAiba, et al., Redox-sensitive regulation of the HIF pathway under non-hypoxic conditions in pulmonary artery smooth muscle cells, Biological Chemistry, 385 249 2004.
[41] N. Gao, et al., Vanadate-induced expression of hypoxia-inducible factor 1α and vascular endothelial growth factor through phosphatidylinositol 3-kinase/Akt pathway and reactive oxygen species, J. Biol. Chem. 277 (2002) 31963–31971.
[42] D.E. Richard, E. Berra, J. Pouysségur, Non-hypoxic pathway mediates the induction of hypoxia inducible factor 1 alpha (HIF-1α) in vascular smooth muscle cells, J. Biol. Chem. 275 (35) (2000) 26765–26771, https://doi.org/10.1074/jbc.M003325200 PMID: 10837481.
[43] N. Feng, et al., HIF-1α and HIF-2α induced angiogenesis in gastrointestinal vascular malformation and reversed by thalidomide, Sci. Rep. 6 (2016) 27280.
[44] G. Hen, et al., Venous-derived angioblasts generate organ-specific vessels during zebrafish embryonic development, Development (Cambridge, England) 142 (2015) 4266.
[45] V. Chandrasekaran, C. Lea, J.C. Sosa, D. Higgins, P.J. Lein, Reactive oxygen species are involved in BMP-induced dendritic growth in cultured rat sympathetic neurons, Mol. Cell. Neurosci. 67 (2015) 116–125.
[46] H. Wang, et al., Cellular hypoxia promotes heterotopic ossification by amplifying BMP signaling, J. Bone Miner. Res. 31 (2016) 1652–1665.
[47] L. Carvalho, C.-P. Heisenberg, The yolk syncytial layer in early zebrafish development, Trends Cell Biol. 20 (2010) 586–592.
[48] A. Donovan, et al., Positional cloning of zebrafish ferroportin1 identifies a conserved vertebrate iron exporter, Nature 403 (2000) 776–781.
[49] E.A. Zemskov, et al., Biomechanical Forces and Oxidative Stress: Implications for Pulmonary Vascular Disease, Antioxidants & Redox Signaling, 2019.
[50] K. Brassington, S. Selemidis, S. Bozinovski, R. Vlahos, New frontiers in the treatment of comorbid cardiovascular disease in chronic obstructive pulmonary disease, Clin. Sci. 133 (2019) 885.
[51] S. Steven, et al., Pentaerythritol tetranitrate in vivo treatment improves oxidative stress and vascular dysfunction by suppression of endothelin-1 signaling in monocrotaline-induced pulmonary hypertension, Oxidative Med. Cell. Longevity 2017 (2017) 4353462-4353462.
[52] V. Tseng, R.L. Sutliff, C.M. Hart, Redox Biology of Peroxisome Proliferator-Activated Receptor-γ in Pulmonary Hypertension, Antioxidants & Redox Signaling, 2018.
[53] B. Poljsak, D. Šuput, I. Milisav, Achieving the balance between ROS and antioxidants: when to use the synthetic antioxidants, Oxidative Med. Cell. Longevity 2013 (2013) 956792-956792.
[54] A. van der Vliet, Y.M.W. Janssen-Heininger, V. Anathy, Oxidative stress in chronic lung disease: from mitochondrial dysfunction to dysregulated redox signaling, Mol. Asp. Med. 63 (2018) 59–69.